COGEAR

MODULE 2:

Identification of potential faults in the Valais

Del. No.: 2a.1.3

Author: Baumann C.

Swiss Seismological Service

SED/COGEAR/R/010/20120712
July 12, 2012

Project Report: COGEAR, Module 2

Task 2a.1.3 Identification of potential faults in the Valais

Cyrill Baumann

I INTRODUCTION: MOTIVATION AND KEY QUESTIONS

The Valais area in the Swiss Alps shows the largest seismic hazard in Switzerland. During the past 500 years, the Valais region experienced six earthquakes around magnitude 6 or larger. Those earthquakes occurred with a periodicity of about 100 years, the most recent one in 1946.

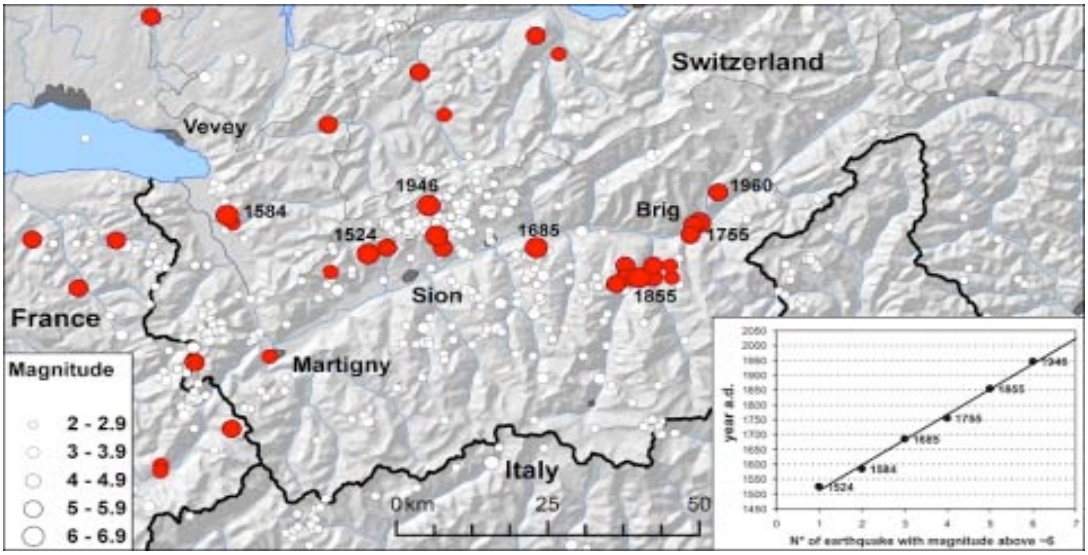

Figure 1 : Area of Valais with some prominent earthquakes during the last 500 years. Red dots point out earthquakes with magnitudes larger than 4, white dots show earthquakes with magnitudes less than 4. The box on the bottom right shows cumulative number of earthquakes.

The Valais presents rough topography, unstable and steep slopes, deep sediment-filled valleys and wide glacier- and snow-covered areas that potentially increase the seismic risk level due to earthquake-induced phenomena such as strong site- and topographical effects, liquefaction, landslides and snow avalanches. In addition, important critical facilities of Switzerland, such as hydroelectric power plants (e.g. Grande Dixence) and chemical plants (Lonza, Syngenta) have been built in the Valais, making the region even more vulnerable to damaging earthquakes. Motivated by this fact, within the framework of the COGEAR project (an interdisciplinary natural hazard project for investigating the hazard induced by earthquakes), we developed a suite of earthquake source physics-based dynamic rupture models consistent with the expected earthquakes in a particular region . Stress distribution prior to earthquakes are assumed to be stochastic with heterogeneous stress consistent, in a statistical sense, with past earthquakes. Evaluation of the current seismic activity and seismotectonics in the area suggests normal fault and strike-slip as potential fault mechanisms. Evidences of the existence of a fault are deduced from the spectral signatures of seismic ambient noise recorded during a seismic survey along the expected fault. These seismological observations together with geological evidences and observed instrumental seismicity are used to constraint the fault location, size and mechanism of our model. The ground motion modeled from the simulated earthquakes are adequately treated to assess the level and variability of ground motion in the area for seismic hazard and risk mitigation, particularly to contribute to the evaluation of critical structures and to improve seismic safety of future and existing structures in the study area.

Some key questions we want to answer are: What are the extreme limits in terms of expected ground-motions, focusing on the expected earthquake magnitudes of about Mw=6.5? Furthermore, we want to investigate how peak ground acceleration (PGA), peak ground velocity (PGV) and peak ground displacement (PGD), particularly in the near field (<30Km), behave. How do shear and normal stress heterogeneities affect the different stages of faulting process and ground motion? How do the evaluated earthquake physics models affect observable quantities such as ground motion patterns?

II FAULT DETECTION IN VALAIS

2.1 FAULTS IN VALAIS: WHAT WE KNOW SO FAR AND WHAT WE CAN EXPECT

(Kastrup, Zoback et al. 2004) give insights into the predominant fault mechanism in the area of Valais. They analyzed systematically the state of stress of the central European Alps and northern Alpine foreland in Switzerland based on focal mechanisms of 138 earthquakes with magnitudes between 1 and 5. Their investigations revealed a predominantly normal faulting and strike-slip to normal faulting regime in the area of Valais.

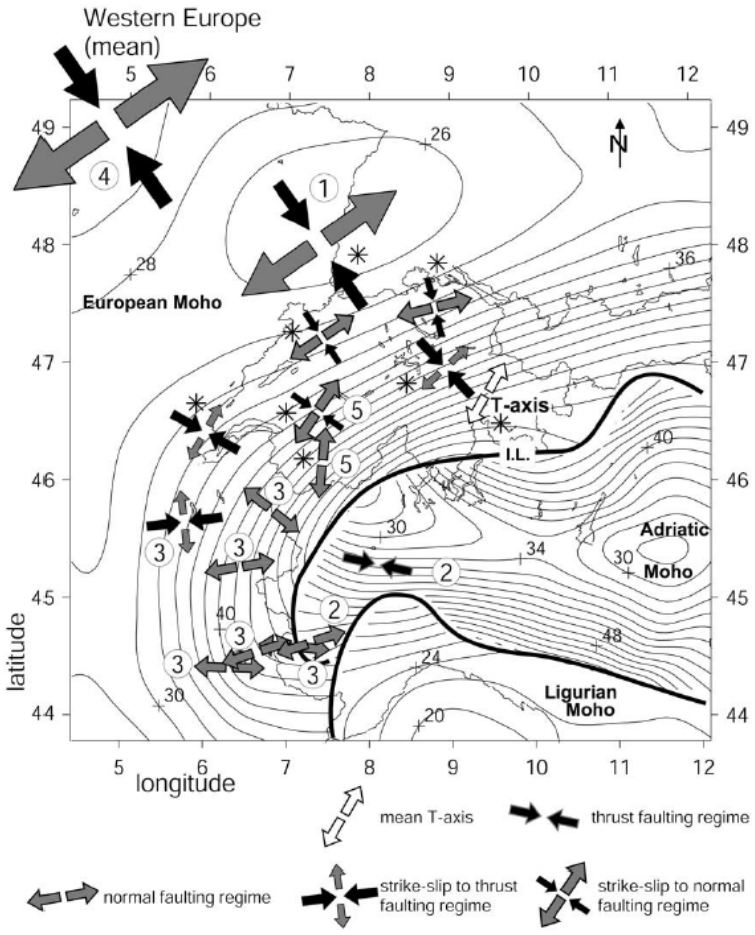

Figure 2: Summary of stress state determinations from the study of (Kastrup, Zoback et al. 2004) and other studies shown with the depth to Moho in the Alpine region after (Waldhauser, Kissling et al. 1998). The contour interval is 2Km. Stress determinations without a number are from (Kastrup, Zoback et al. 2004).

(Campani 2009) investigated the Simplon fault, which is probably the largest fault in Switzerland. The Simplon fault consists of the Rhone line, which is a strike-slip fault striking along the Rhone valley and transforming then near Visp into the Simplon line, a normal faulting system. The Simplon line has a shallow dip (around 30°), strikes generally NW-SE, and has a length of about 30 Km.

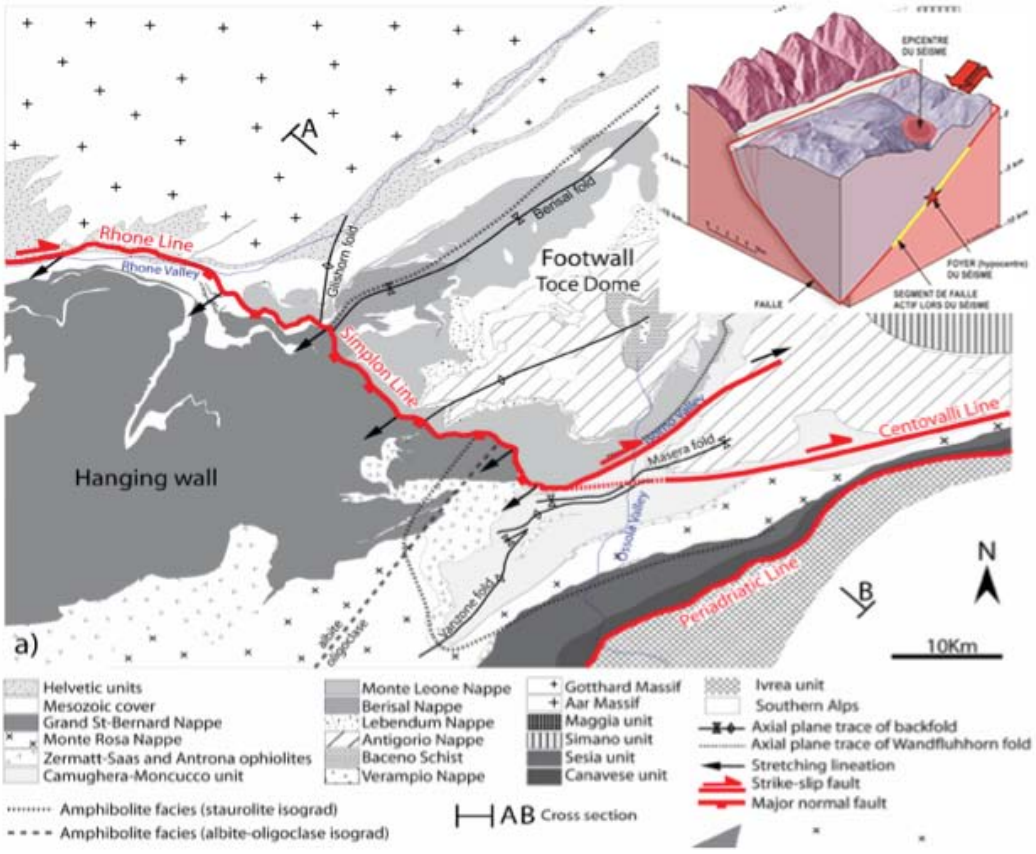

Figure 3: Simplon fault, consisting of the Rhone , Simplon and Centovalli line. The SE-continuation of the Simplon fault is not that clear so far. The Rhone line is a dextral strike-slip fault which transforms near Visp into a normal fault (Simplon line). The Centovalli line seems to be again a right lateral strike-slip fault. *Block diagram top right*: Shown is the area of Visp. The large valley is the Rhone valley, the small one is the valley of Visp. Along the Rhone valley, strike-slip is dominating. In the region of Visp, there is a transformation between strike-slip and normal faulting. The star indicates the hypocenter of the 1855 Visp earthquake which had a moment magnitude of 6.4. The block diagram is according to M.Sartori (www.crealp.ch). Figure after (Campani 2009).

Some authors (e.g. M. Sartori) think, that the Simplon line could have caused the 1855 Visp earthquake, which had a moment magnitude Mw = 6.4 (Kozák and Vaněk 2006). In context of NFP 20, it was possible to verify a west dipping fault in the area of the Visp valley.

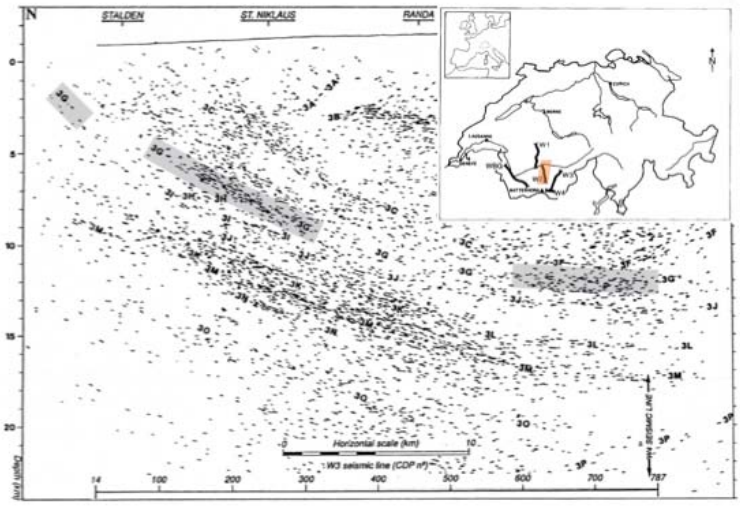

Figure 4: Results from NFP20 (Nationales Forschungsprogramm) refraction seismic survey in Switzerland as part of the European Geotraverse EGT project. The Figure shows refraction seismics signatures of a westwards flat dipping structure, which could be a normal fault (Marchant 1993).

Constraints in depth come from (Deichmann 2003). He could show that earthquakes below Alpine region have a maximum depth of about 20 Km. This is possibly because the ductile regime reaches shallower depths under the Alps than under lowland.

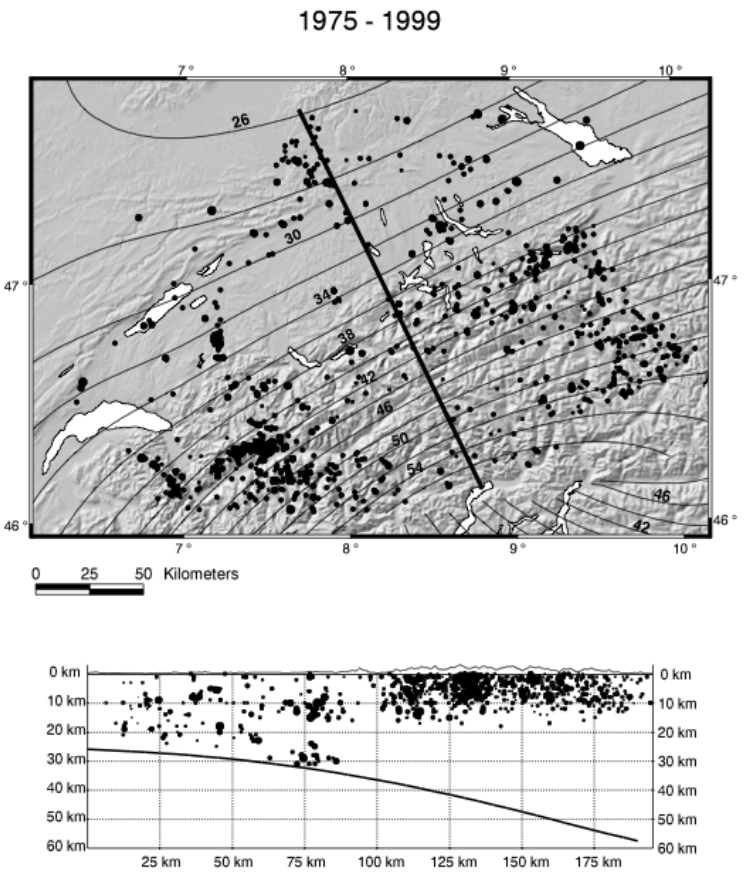

Figure 5: Epicenter map and depth cross-section along a NNW-SSE trending profile from Basel to Locarno of selected earthquakes between 1975 and 1999. Moho topography (Waldhauser 1996) & (Waldhauser, Kissling et al. 1998). Surface topography is from the digital elevation model "RIMINI", reproduced with permission from the Swiss Federal Office of Topography (BA002892), complemented with data from the 30" elevation model (GTOPO30) of the USGS. Figure after (Deichmann 2003).

The papers mentioned above (Kastrup et al. 2002, Campani 2009 and Deichmann 2003) gave us some ideas how we have to model the fault of interest, in order to obtain realistic earthquake scenarios for Alpine regions, particullary in the Valais area. It makes sense to model normal faults or strike-slip faults and considering earthquakes to appear in a depth less than 20 Km.

During the past 500 years, several earthquakes with magnitudes 6 and larger stroke the area of Visp. The maximum magnitude was Mw=6.4 during the 1855 Visp earthquake. In the following part, we try to estimate the fault dimensions on the base of the Visp 1855 earthquake. We use the empirical relationship of (Wells and Coppersmith 1994) in order to obtain an idea of the fault dimensions we can expect, a fault which is capable to produce earthquakes with moment magnitudes of Mw=6.4.

$$A = 10^{(-2.87+0.82 \cdot Mag)} \qquad (1)$$

Relationship (1) is valid for normal faulting. If we assume a square fault with length *l* and a moment magnitude Mw=6.4, then we obtain a fault size of about 240.25 Km^2.

In summary, we can state, that it seems to be reasonable to model normal faults and strike-slip faults with lengths around 12 Km and widths around 20 Km to appropriately model earthquakes in the region of Visp which is representative for Alpine regions. There are some issues about the orientation

of the faulting regarding to the stress distribution according to (Kastrup, Zoback et al. 2004) which have to be clearafied.

Being aware of the fault we are looking for (using the moment magnitude of the Visp 1855 earthquake, Mw=6.4), a normal or strike-slip fault with a length around 12 Km and a width of about 20 Km, we tried to find indications for the fault, on which the 1855 Visp earthquake occurred. There are several indications for a fault and/or fault-system in the region of Visp:

- *The Simplon fault in the area of Visp could be a candidate for the origin of the 1855 Visp earthquake*
- *The damage field of the 1855 Visp earthquake shows the strongest damages in the approximity of Visp (Fritsche 2008)*
- *Field observations of coseismic displacement: 20-30cm in the vineyard between Visp and Unterstalden. An observation which was made by a local geologist (C.L. Joris).*
- *Geological field observations (Werenfels 1924) of a „Querbruch" between Unter- and Oberstalden.*
- *Observations of the Hotee fault in the tunnel construction area Eyholz*
- *Observations of a potential fault near Stalden, made by ETH geologist (J. Moore). This observation could be the southern continuation of the Visp-1855-fault.*

As already mentioned, the fault could have a dimension of about 12x20 Km. In comparison, the distance between Visp and Stalden is about 7.5 Km (Figure 6).

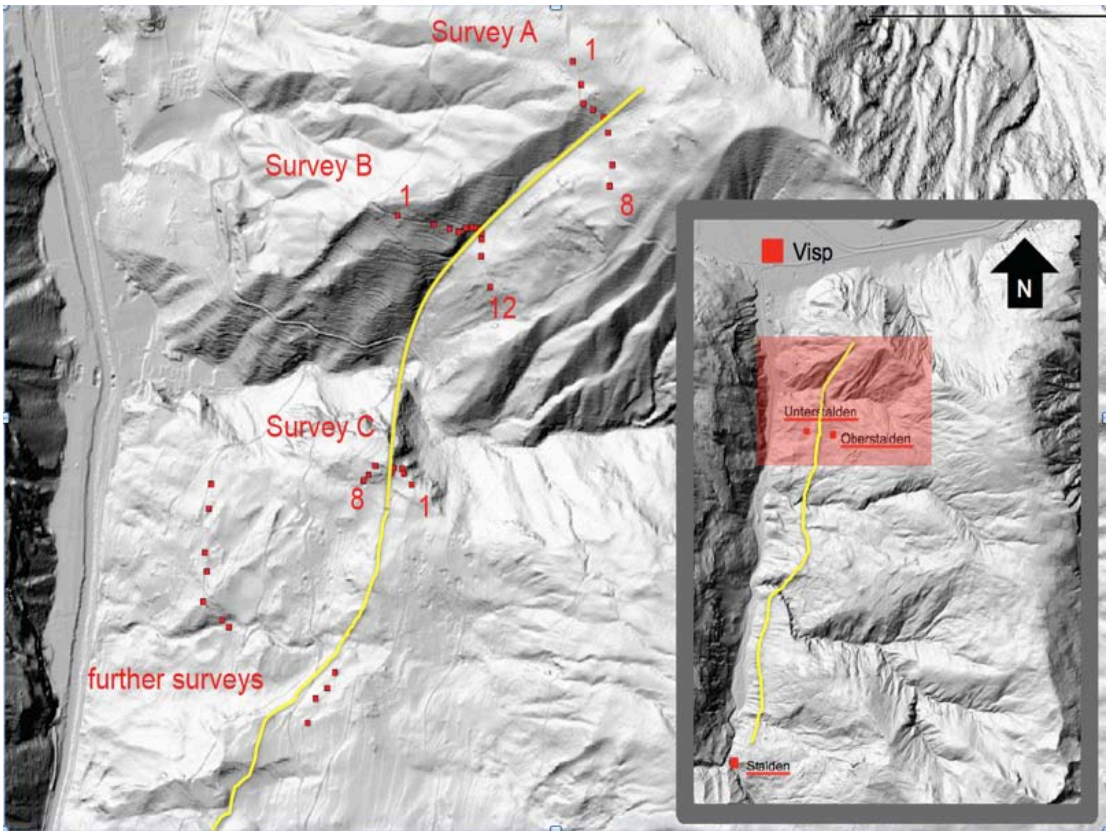

Figure 6: Investigation area valley of Visp, where we assume the 1855 Visp fault which is in turn most likely part of the Simplon line. The grey framed box right shows the Vispertal (Visp to Stalden, which is about 7.5 Km), the investigation area (redish shaded) and the assumed fault line (yellow line). The main map shows again the supposed fault line (yellow) as well as the three principal survey lines (A, B and C). Small red squares are standing for seismometers. We performed further surveys southeast and southwest of survey C, but we could not find any seismic anomalies there.

2.2 USING AMBIENT NOISE TO LOCATE FAULTS

We applied a passive seismic investigation method which is based on the assumption that a fault is surrounded by fracturized rock shown in Figure 7.

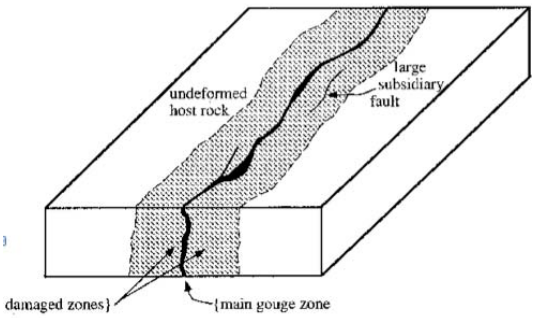

Figure 7: Generalized fault zone structure showing main gauge zone along which most fault displacement occurs, surrounded by damaged rock, charcterized by subsidiary deformational features (faults, fractures, cataclasis, and surrounding undeformed host rock (Chester and Logan 1986).

When seismic waves penetrate the gauge zone, energy is absorbed (e.g. heat), which leads to a decrease in amplitude of the seismic wave. The loss of energy also leads to a decrease of seismic velocity. The gauge zone, the zone in which the seismic velocity is reduced, is called low velocity zone (LVZ). The attempt is to detect reduced amplitudes in the seismic traces which could be an indicator for a LVZ.

Passive seismic methods are cheap and easy to perform. The seismic source is given by ambient noise which is generated in the region of Visp as followed (Michel 2010, presonal communication)

- *<1 Hz* *natural (e.g. tides)*
- *2-10 Hz* *mainly Lonza (chemical company)*
- *10-25 Hz* *road traffic*
- *>25 Hz* *close traffic, especially trains*

We performed several seismic surveys during day and night. Usually we measured about 3 hours. The number of sensors was in average 10. The data acqusition was carried out with LE-3D/5s seismometer sensors and digitized with Quanterra Q330.

The data were subjected to a spectral analysis, using a Fortran 90 library for multitaper spectrum analysis, provided by (Prieto, Parker et al. 2009). In the multitaper method, the data sequence to be analyzed is multiplied by a series of weights called tapers, the result is then Fourier transformed (using FFT) and squared to obtain the estimate of the power spectral density (PSD). These tapers are selected to optimally minimize broad-band bias, the tendency for power from strong peaks to spread into neighbouring frequency intervals of lower power (spectral leakage).

When we performed the measurements, the alignement of the seismometers was north. During the data processing phase we rotated the north direction such that it was aligned with the fault normal. But actually, the differences between the spectra of the north and the fault normal alignement was small.

The topography of the investigation area is fairly rough which made it difficult to place the seismometers. Therefore we decided to place the seismometers along adequate roads which made it easy to arrange the array. The disadvantage was that we had a lot of noise coming from passing vehicles. This additional noise manifests itself in strong peaks in the seismic spectra especially during day measurements. Therefore, for the analysis it was important to avoid parts of the traces in which we had too strong peaks. For this purpose, we took different time windows and compared the results. Figures 8 and 9 show the choice of a time window in case of Survey A (Figure 6).

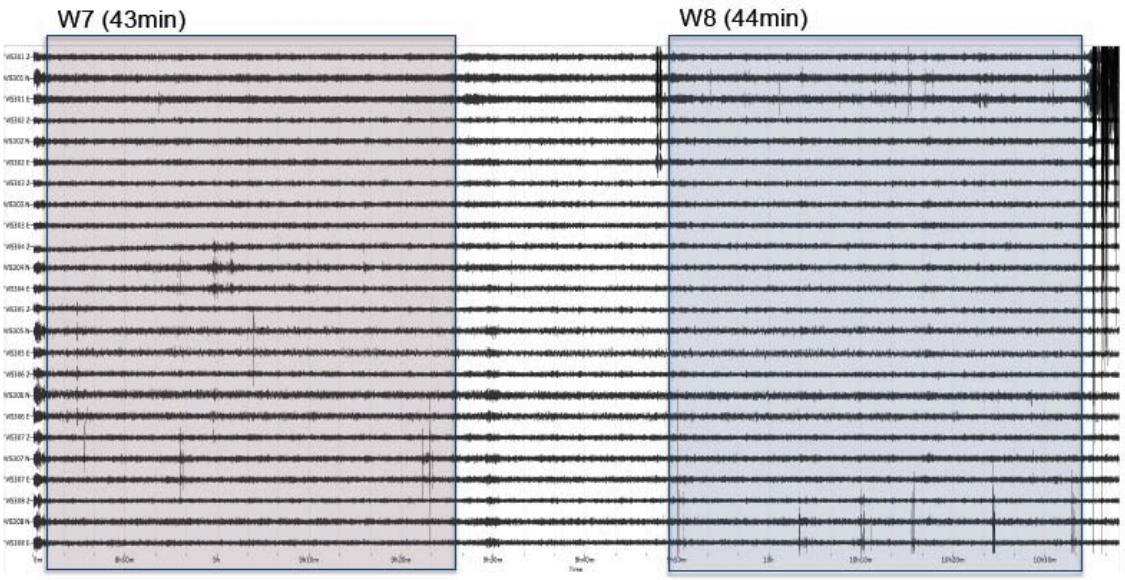

Figure 8: Recordings of 8 seismometers forming Survey A. The y-axis shows 3 components (N, E and Z) for each seismometer, the x-axis shows time in hours and minutes. W7 (43 min) and W8 (44min) are different time windows, selected by eye, containing as small variations as possible. The power spectra gained from those data are shown in Figure 9.

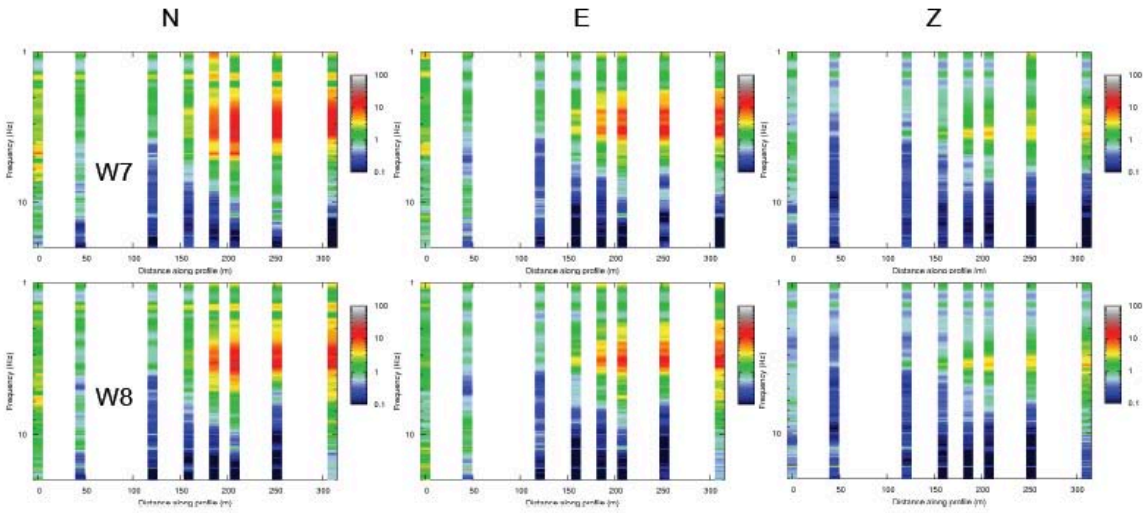

Figure 9: Power spectra resulting from time window 7 (W7) and 8 (W8). N, E and Z mean north, east and vertical component. Y-Axis means frequency from 1 to more than 10 Hz. The results show that the overall pattern (area of high amplitudes in red and area of low amplitudes in blue) does weakly depend on the chosen time window, especially in this case (Survey A).

We considered in Survey A, B and C different time windows and found that for our purposes, the choice of time window has an insignificant impact on the power spectra. We also had a look for the H/V-ratios, which were not revealing.

2.3 SEISMIC SURVEYS

The results of seismic surveys are shown in the following on the base of normal components of Survey A, B and C. The power spectra of Survey A, B and C show a clear coherent seismic anomaly which is characterized by a reduction of the amplitudes.

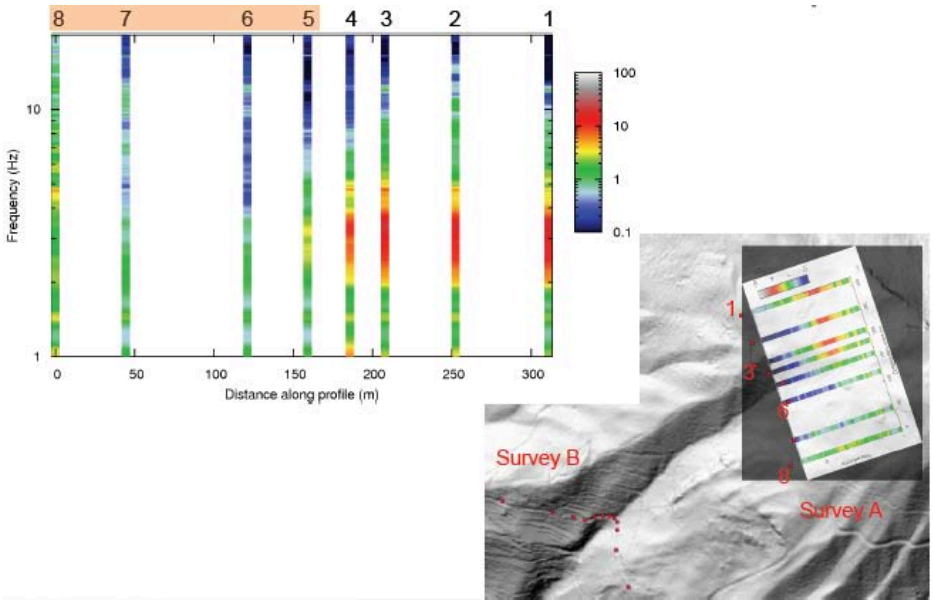

Figure 10: Power spectrum of Survey A. The map section on the right side shows the spectrum relative to the topography. The x-axis of the power spectrum shows the distance along profile in meters. Each bar stands for a seismometer (which is numbered on the top: 1-8). Y-axis means frequency. The amplitudes are reduced for stations 5 to 8. The color bar shows the wave amplitude: blue means low and red high amplitude.

For all Surveys (A, B and C) we see that there is no modification for low frequencies (below 2Hz). But frequencies higher than 2Hz are modified. Figure 10 shows a clear reduction of the amplitudes in case of survey A for frequency ranges higher than 2Hz. The strongest amplitude decay is found at stations 5, 6, 7 and 8.

In Figure 11, we have the power spectrum of Survey B. Here we have the strongest amplitude reduction for frequencies between 1 and around 10Hz, particulary strong in the couloir around station 7.

The results of Survey C are shown in Figure 12. At the seismometers 3, 2 and 1, we have clearly reduced amplitudes.

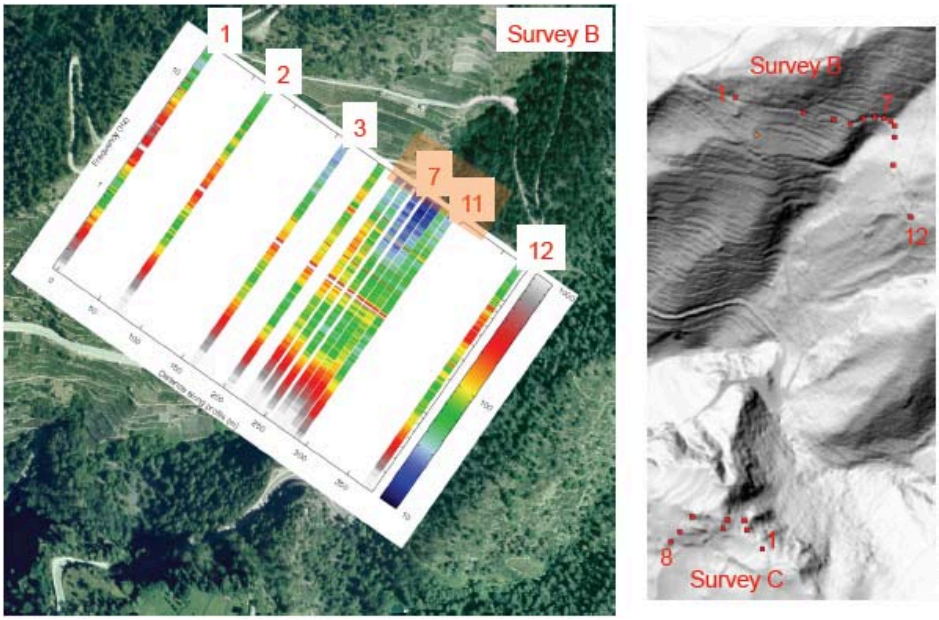

Figure 11: Power spectrum of Survey B. The map section on the right side shows the topography. The x-axis of the power spectrum shows the distance along profile in meters. Each bar stands for a seismometer (which is numbered on the top: 1-12). Y-axis means frequency. The amplitudes are reduced around 7. The color bar shows the wave amplitude: blue means low and red high amplitude.

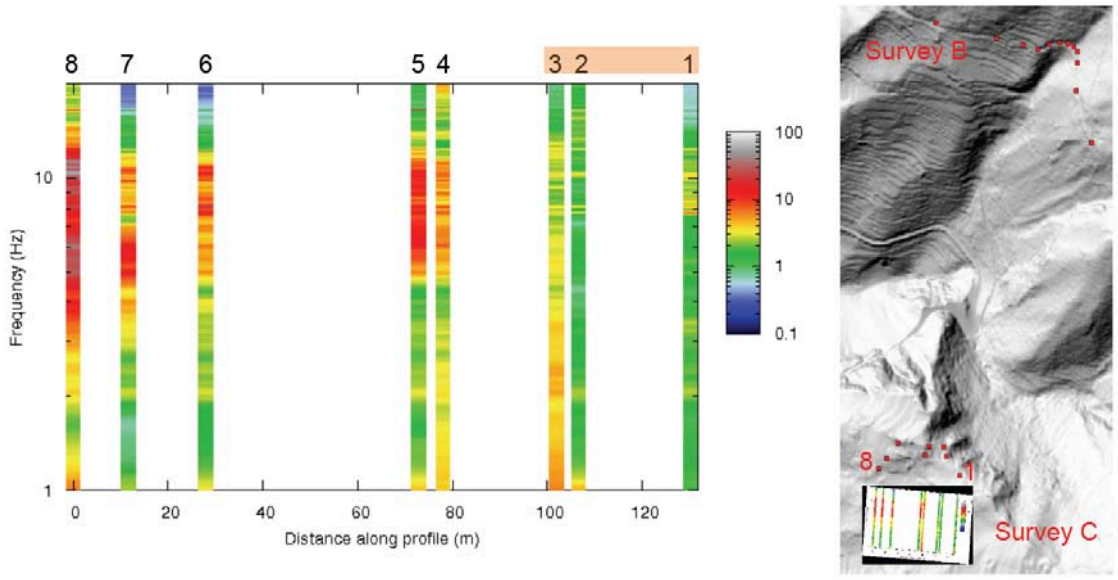

Figure 12: Power spectrum of Survey C. The map section on the right side shows the spectrum relative to the topography. The x-axis of the power spectrum shows the distance along profile in meters. Each bar stands for a seismometer (which is numbered on the top: 1-8). Y-axis means frequency. The amplitudes are reduced for stations 1 to 4 . The color bar shows the wave amplitude: blue means low and red high amplitude.

This seismic anomaly expressed in the amplitude reduction, is observed in all components of the spectrum, it is therefore likely that we have found a real feature.

Geological data support the results of the seismic surveys. The construction of the Eyholz tunnel and a geological map of (Werenfels 1924) encourage our efforts in the investigation area. (Werenfels 1924) mapped a cross fault near Oberstalden which is in a quite good agreement with the recordings of stations 1, 2 and 3 of Survey C. Where Werenfels mapped 1924 the fault, we have found reduced amplitudes in the power spectrum (Figure 13).

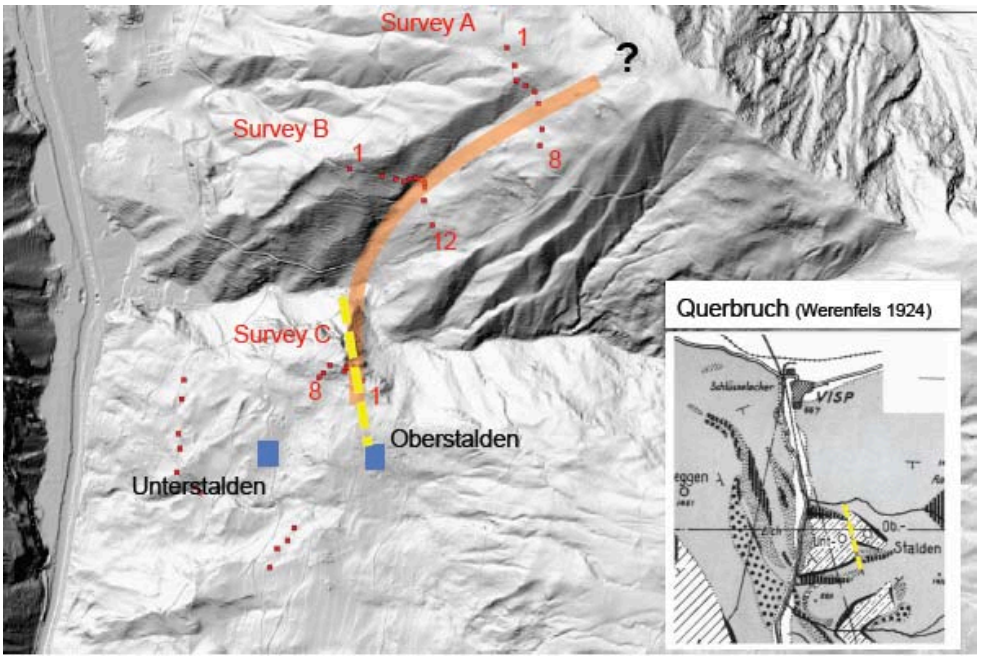

Figure 13: The inset shows a geological map of (Werenfels 1924). In Yellow, the observed fault situated between Unter- und Oberstalden is assigned. The large Figure shows in orange the assumed fault and in yellow the fault reported by Werenfels.

Geologists from the construction site Eyholz mapped a dominant feature, so called Hotee-Störung, in the tunnel. This fault could be connected with the fault which was reported by (Werenfels 1924) The anomaly we recorded, at least in the context of Survey C, seems to be a real feature – observed at the surface (Werenfels 1924) and in the depth (tunnel).

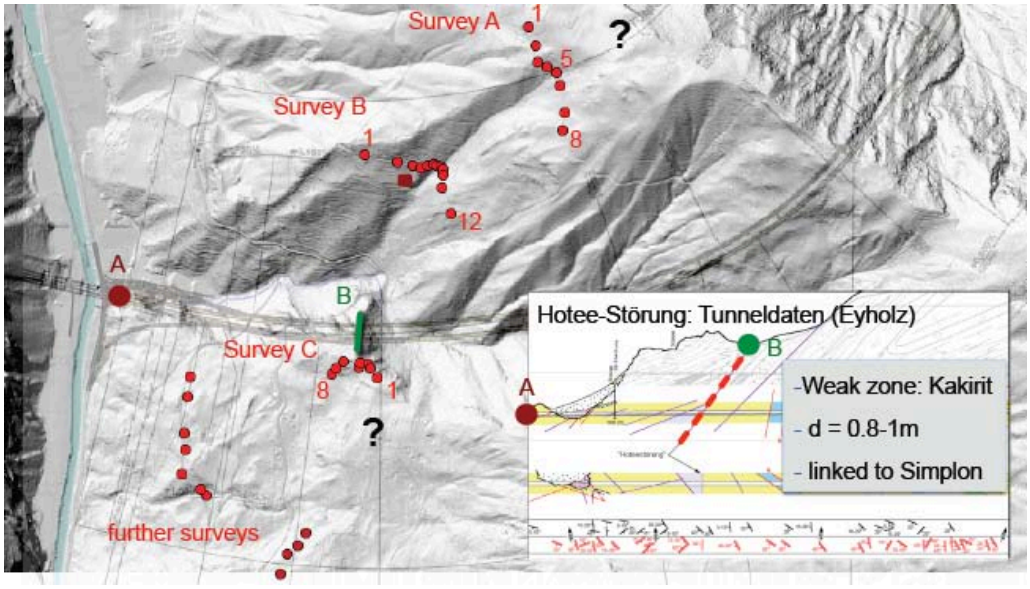

Figure 14: The inset shows a vertical section of the Eyholz tunnel, beginning in Staldenbach (point A). The large figure shows the tunnel line and in point B the theoretical outcrop of the Hotee fault. Kakirit forms the Hotee-fault, which has a diameter between 0.8 and 1m.